

# The Properties of Cataclysmic Variables In Photometric $H\alpha$ Surveys

A. R. Witham,<sup>1</sup> C. Knigge,<sup>1</sup> B. T. Gänsicke,<sup>2</sup> A. Aungwerojwit,<sup>2</sup>  
R. L. M. Corradi,<sup>3,4</sup> J. E. Drew,<sup>5</sup> R. Greimel,<sup>3</sup> P. J. Groot,<sup>6</sup>  
L. Morales–Rueda,<sup>6</sup> E. R. Rodríguez–Flores,<sup>4,7</sup> P. Rodríguez–Gil,<sup>4</sup>  
and D. Steeghs.<sup>8</sup>

<sup>1</sup> School of Physics & Astronomy, University of Southampton, Highfield, SO17 1BJ, U.K.

<sup>2</sup> Department of Physics, University of Warwick, Coventry CV4 7AL, U.K.

<sup>3</sup> Isaac Newton Group of Telescopes, Apartado de correos 321, E-38700 Santa Cruz de la Palma, Tenerife, Spain

<sup>4</sup> Instituto de Astrofísica de Canarias, 38200 La Laguna, Tenerife, Spain

<sup>5</sup> Imperial College of Science, Technology and Medicine, Blackett Laboratory, Exhibition Road, London, SW7 2AZ, U.K.

<sup>6</sup> Afdeling Sterrenkunde, Radboud Universiteit Nijmegen, Faculteit NWI, Postbus 9010, 6500 GL Nijmegen, the Netherlands

<sup>7</sup> Instituto de Geofísica y Astronomía, Calle 212, No. 2906, CP 11600, La Habana, Cuba

<sup>8</sup> Harvard-Smithsonian Center for Astrophysics, 60 Garden Street, Cambridge, MA 02138, USA

2005 August 5

## ABSTRACT

We report on the properties of 71 known cataclysmic variables (CVs) in photometric  $H\alpha$  emission line surveys. Our study is motivated by the fact that the Isaac Newton Telescope (INT) Photometric  $H\alpha$  Survey of the northern galactic plane (IPHAS) will soon provide  $r'$ ,  $i'$  and narrow-band  $H\alpha$  measurements down to  $r' \simeq 20$  for all northern objects between  $-5^\circ < b < +5^\circ$ . IPHAS thus provides a unique resource, both for studying the emission line properties of known CVs and for constructing a new CV sample selected solely on the basis of  $H\alpha$  excess. Our goal here is to carry out the first task and prepare the way for the second. In order to achieve this, we analyze data on 19 CVs already contained in the IPHAS data base and supplement this with identical observations of 52 CVs outside the galactic plane.

Our key results are as follows: (i) the recovery rate of known CVs as  $H\alpha$  emitters in a survey like IPHAS is  $\simeq 70$  per cent; (ii) of the  $\simeq 30$  per cent of CVs which were not recovered  $\simeq 75$  per cent were clearly detected but did not exhibit a significant  $H\alpha$  excess at the time of our observations; (iii) the recovery rate depends only weakly on CV type; (iv) the recovery rate depends only weakly on orbital period; (v) short-period dwarf novae tend to have the strongest  $H\alpha$  lines. These results imply that photometric emission line searches provide an efficient way of constructing CV samples that are not biased against detection of intrinsically faint, short-period systems.

**Key words:** surveys – binaries: close – novae, cataclysmic variables

## 1 INTRODUCTION

Cataclysmic variables (CVs) are interacting binary systems in which a white dwarf (WD) primary accretes matter from a main-sequence secondary via Roche lobe overflow. If the magnetic field of the WD is dynamically unimportant, the accretion process takes place entirely via a disc surrounding the WD. By contrast, if the magnetic field is very strong, the accretion stream from the secondary is channelled directly onto the magnetic poles of the WD. Finally, in the interme-

diated range of field strengths, a partial disc may form that is truncated on the inside by the WD magnetic field.

An observational feature that is common to all of these different accretion modes are (Balmer) emission lines. In weakly-magnetic CVs, the observed line emission may originate from optically thin or irradiated parts of the accretion disc (Williams 1980). In magnetic CVs, line emission may be produced in the accretion stream, any residual accretion disc, or in the so-called accretion curtains that channel material from the inner edge of a truncated disc to the

magnetic poles of the WD. The irradiated secondary star in CVs can also contribute an appreciable contribution to the observed line emission, particularly in polars. Warner (1995) provides a comprehensive review of CVs, including their spectroscopic properties.

Given the ubiquity of line emission amongst CVs, emission line surveys offer a powerful way to find new CVs (for a current example of such a CV search, see Gänsicke et al. 2002 and Aungwerojwit et al. 2005). What makes this strategy particularly promising is that, empirically, the intrinsically faintest, low mass transfer rate ( $\dot{M}$ ) systems tend to have the largest Balmer line equivalent widths (EWs; Patterson 1984). Population synthesis models suggest that such low accretion rate systems should totally dominate the galactic CV population and should be found predominantly at short orbital periods, that is below the well-known CV “period gap” between 2.2 hrs and 2.8 hrs (Kolb 1993; Howell et al. 1997). However, this dominant population of faint, short-period CVs has proven quite elusive, and it is still not clear whether this is due to selection effects or whether it points to a serious flaw in our understanding of CV evolution. Since emission line surveys should be very good at finding low  $\dot{M}$  CVs, they should be an excellent way of detecting the large population of faint, short-period CVs, if it exists.

The INT/WFC Photometric H $\alpha$  Survey of the northern galactic plane (IPHAS) is currently surveying the Milky Way in  $r'$ ,  $i'$  and H $\alpha$  and provides an excellent data base for a detailed CV search at low galactic latitudes. The survey goes to a depth of  $r' \simeq 20$  and covers the latitude range  $-5^\circ < b < +5^\circ$ . A detailed introduction to the survey is given by Drew et al. (2005).

In this paper, we investigate the properties of the known population of CVs that have been observed by IPHAS, supplemented with additional observations of CVs outside the galactic plane with the IPHAS set-up. Such a study is useful for two main reasons. First, it allows us to determine the recovery rate of CVs as H $\alpha$  emitters as a function of CV subclass, orbital period and apparent magnitude. These recovery rates effectively specify the completeness of the survey with respect to CVs, which is crucial for the interpretation of the new CV sample that is currently being constructed based on IPHAS data. Second, the existence of a large, uniform sample of broad- and narrow-band magnitudes for known CVs allows us to check for and update correlations between key observables (for example H $\alpha$  excess) and intrinsic CV parameters (for example orbital period and absolute magnitude).

The structure of this paper is as follows. Section 2 discusses the observations obtained. Section 3 discusses the two CV samples analysed in the paper and how they have been observed. The techniques for selecting CVs from photometric data are presented in section 4. In section 5, we present and discuss our estimates for CV recovery/detection rates with IPHAS-like emission line surveys. In section 6, we consider correlations between key observables and system parameters. Our findings are discussed in section 7, focusing particularly on the ability of IPHAS to uncover the long-sought population of faint, short-period CVs. We summarize our conclusions in section 8.

## 2 OBSERVATIONS

Our study relies on two observational data sets. The first is composed of the IPHAS galactic plane observations that were completed up to and including July 2004; this amounts to about 1/3 of the final survey area. The second consists of a series of imaging observations obtained in June 2004 of northern CVs with galactic latitudes  $|b| > 5^\circ$ . Both datasets were obtained with the same instrumental set-up and observing strategy, and both were reduced with the standard IPHAS pipeline.

Full details of the IPHAS observing strategy and reduction procedures may be found in Drew et al. (2005). Briefly, all observations were obtained using the Wide Field Camera (WFC) on the Isaac Newton Telescope, which gives a spatial pixel size of  $0.333'' \times 0.333''$  over a field of view of approximately 0.3 square degrees. Photometry was carried out using a set of three filters, comprising a narrowband H $\alpha$  filter and an additional set of two broadband Sloan  $r'$  and  $i'$  filters. Exposure times were 120s for the H $\alpha$  images, 10s for the  $i'$  band images, and 10s [30s] seconds for all  $r'$  band images obtained before [after] June 2004. Finding charts from Downes et al. (2001) were used to identify the CVs in our images.

The final IPHAS data base will contain only observations that meet a strict set of quality constraints. However, in order to avoid restricting our CV sample too much in the present analysis, we did not limit ourselves to fields that have passed the IPHAS quality controls. Instead, for each CV, we simply took the data from the best available set of observations.<sup>1</sup> Thus some of the data analysed here will not be included in the final published survey catalogues. Instances in which the data quality of a field was below the nominal limits will be indicated explicitly. However, our results from these fields are consistent with the results from fields with data quality that passes the IPHAS quality controls.

We finally note that, in all of our analysis below, we only work with sources brighter than a pre-defined magnitude limit of  $r' = 19.5$ . In principle, IPHAS goes somewhat deeper than this, to about  $r' \simeq 20$ . However, the increased photometric scatter exhibited by the very faintest sources makes it counter-productive to include these sources in our selection algorithm (see Section 4).

## 3 CONSTRUCTION OF CV SAMPLES

As noted above, the data we use in our study come from two distinct sources. The first is the standard IPHAS database, the second is a set of observations of CVs at higher galactic latitudes observed with the IPHAS set-up. The majority of the fields in the second data set exhibit a significantly lower object density than the IPHAS fields. This may be expected to affect CV recovery rates, and we therefore retain the distinction between In-Plane and Off-Plane samples in our study.

<sup>1</sup> Note that a given CV can be present in multiple IPHAS pointings because (i) most locations are observed at least twice with the IPHAS tiling pattern, and (ii) poor quality observations may already have been repeated.

### 3.1 The In-Plane CV Sample

Adopting a limiting magnitude of  $r' = 19.5$  the IPHAS imaging database as of July 2004 contains 19 known cataclysmic variables<sup>2</sup> listed in the Ritter & Kolb catalogue (Ritter & Kolb 2003)<sup>3</sup>. We extracted standard IPHAS catalogues, containing object positions and magnitudes, for all of the IPHAS fields that include these CVs. As noted above, when multiple observations were available for a given CV, we always worked with data from the field observed under the best conditions. Information and data on each CV in the sample are listed in Table 2. This includes a flag to mark data that were extracted from fields that do not meet the nominal IPHAS quality thresholds.

### 3.2 The Off-Plane CV Sample

The targets for off-galactic-plane ( $|b| > 5^\circ$ ) observations were again chosen from Ritter & Kolb (2003), with the main additional constraint being that the target should be observable in June 2004. A sample of 52 Off-Plane CVs turned out to satisfy our magnitude limit of  $r' < 19.5$ . The IPHAS pipeline-reduced data were extracted in exactly the same way as for the In-Plane CVs.

One target, the dwarf nova (DN) IY UMa, deserves additional comment. It was found to have a faint close companion which is not identified in the finding charts and has not been previously described in literature. In the  $r'$  band, the faint companion has a magnitude of 19.27 mag and is separated from IY UMa by 3.5 arcsec. The faint companion has resulted in IY UMa being detected as an unresolved blend in the  $i'$  band, which makes the  $i'$  band magnitude unreliable in this case.

## 4 SELECTING H $\alpha$ EXCESS OBJECTS

We have developed a systematic selection algorithm to identify H $\alpha$  excess outliers (and hence likely emission line objects) from  $r' - \text{H}\alpha$  vs  $r' - i'$  colour-colour plots of individual fields. The selection process does not require user intervention and allows us to separate the CVs into those that show clear H $\alpha$  emission and those that do not. We can then use this information to test for statistical completeness and selection biases in samples of CVs constructed solely on the basis of photometric H $\alpha$  excess. In the following subsections, we describe the sequence of steps used by our selection algorithm to identify likely emission line sources.

### 4.1 Initial Selection Cuts

The first step in our selection procedure is to apply the following criteria to all objects in the catalog for each field in the IPHAS database. First, objects must be detected in all three photometric bands and must not fall on bad pixels of the CCDs. Second, the objects must have positions in

the three photometric bands that match to within 1 arcsec. Third, objects must be classified as “stellar” in the  $i'$  band, and “stellar” or “probably stellar” in the  $r'$  and H $\alpha$  bands. We allow “probably stellar” classification in  $r'$  and H $\alpha$  to avoid excluding stars surrounded by extended H $\alpha$  nebular emission. This prevents the removal of CVs with nova shells (for example T Aur in our In-Plane sample).

### 4.2 Locating the Main Stellar Locus

Objects surviving the initial cuts are then subjected to an iterative selection algorithm (illustrated in Fig. 1). First, they are divided into four magnitude bins, based on their  $r'$  band magnitudes. Next  $r' - \text{H}\alpha$  versus  $r' - i'$  colour-colour plots are created for each magnitude bin in each field.

We next carry out an initial straight line least squares fit to the objects in each magnitude bin. Objects with strong H $\alpha$  emission lines should exhibit an excess in  $r' - \text{H}\alpha$  and will therefore generally be located above the main stellar loci in the plots. The least squares fit is an initial attempt to fit the main stellar loci, and so we expect H $\alpha$  emitters to reside above the fit in the plot. For fields with low number density, which includes the majority of fields outside the galactic plane, this initial fit to all objects often works well. However, in fields with higher number densities, the stellar locus often splits due to the presence of different stellar populations (giants and dwarfs) and different reddening values (see Drew et al. 2005 for a detailed explanation). The key point for our purposes is that the upper locus of points in the colour-colour plots often runs above the initial least squares fit in fields dominated by more distant/highly reddened population. Thus a selection criterion based solely on an object’s position relative to our initial fit would result in the erroneous selection of many ordinary late-type unreddened main-sequence stars which reside in the upper locus of points.

### 4.3 Identifying The Upper Boundary of the Main Stellar Locus

In order to prevent the selection of unreddened objects with no H $\alpha$  emission, we use an iterative  $\sigma$ -clipping technique to force the fit onto the upper boundary of the main stellar locus. The fact that the unreddened objects reside at the top of the main stellar loci is used in our technique to exclude gradually points below the initial fit line in subsequent iterations. In practice, we use four iterations to arrive at a final best-fit fit to the the upper boundary of the main stellar locus. The final iteration is used to give precedence to objects that are well separated from the initial fit (within reasonable limits) rather than those objects that lie in the regions where the upper boundary of the main stellar locus is no longer clearly separated from the lower regions of the main stellar locus.

However, this final fit may not always be appropriate, such as in fields where the stellar locus is not actually split. In these cases, the gradient of the upper boundary of the main stellar locus fit often matches closely with the initial least squares fit or exhibits a nonphysically large slope. If either of these conditions is met, the selection of H $\alpha$  emitters is based on the initial fit; in all other cases, the final fit is

<sup>2</sup> Note that we omit the double-degenerate AM CVn systems from consideration; these He-rich systems belong to a different evolutionary channel and are not expected to show H $\alpha$  emission.

<sup>3</sup> The Ritter & Kolb catalogue is available online at <http://physics.open.ac.uk/RKcat>.

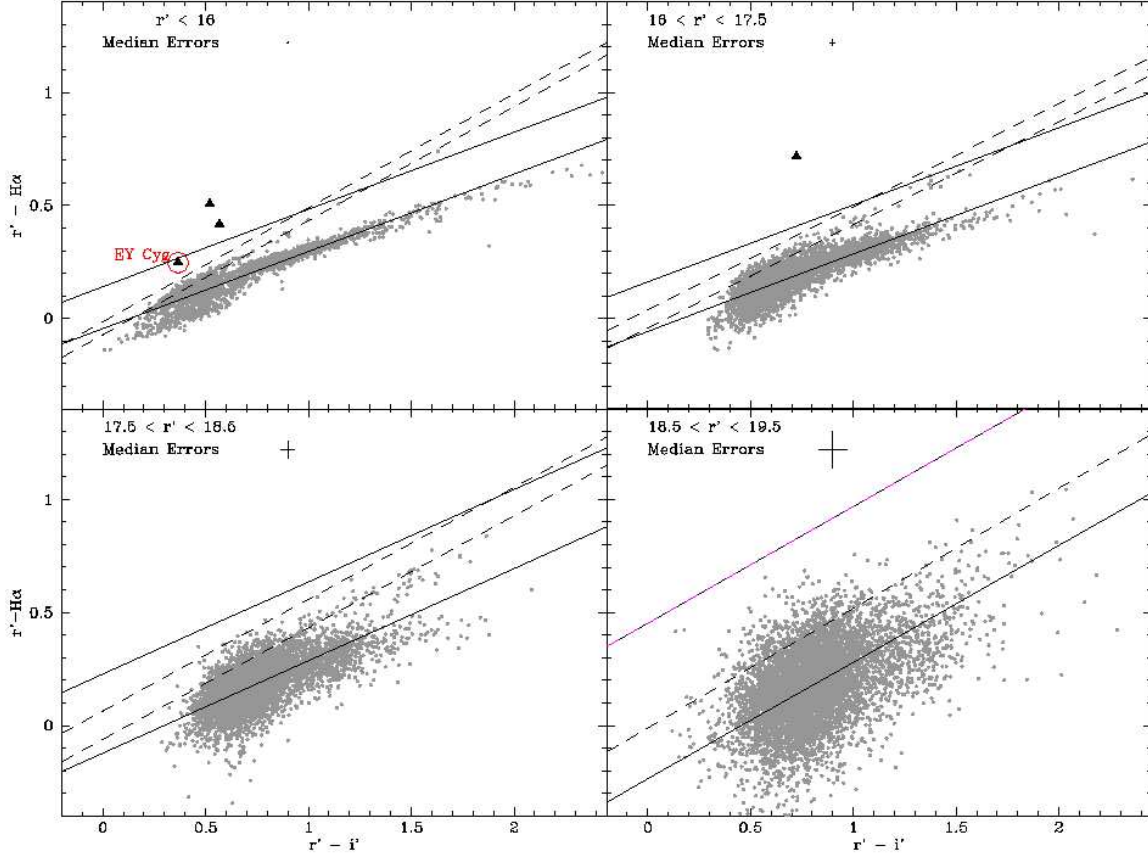


**Figure 1.** An illustration of the selection criteria used to identify strong emission line objects on colour-colour diagrams. The data shown here are all from the IPHAS field 5455 which surrounds the bright dwarf nova EY Cyg. First, the data are split up into four magnitude bins, as shown in the four panels. Objects with H $\alpha$  excess should be located near the top of a colour-colour diagram. The thick lines illustrate the fits to the data, and the thin lines illustrate the corresponding cuts used to single out clear H $\alpha$  emitters. The solid lines show the original least squares fit to the full dataset, along with the corresponding selection cut. The dashed lines show the final fit and cut lines, obtained by applying an iterative  $\sigma$ -clipping techniques to the initial fit. The goal of the  $\sigma$ -clipping is to fit only the upper boundary of the main stellar locus in the colour-colour diagram. Objects selected as H $\alpha$  emitters are shown as large triangles. Note that the cut lines shown here are only approximate, as the actual selection criterion used also considers the errors on each individual datapoint (see Equation 2).

used to select emitters. Empirically, we find that this method gives reasonable results 94 per cent of the time (compared to visual inspection). That is, the fit runs through the upper boundary of the stellar locus when it is visible and otherwise fits the whole stellar locus in a satisfactory manner.

#### 4.4 Selecting H $\alpha$ Excess Objects

Once the appropriate fit for each bin has been decided, we identify objects significantly above the chosen fit as likely H $\alpha$  emitters. Our selection criterion takes into account both the scatter of points around the stellar loci and the errors on the colours of each individual datapoint. We first define the H $\alpha$  excess for each object as

$$\Delta H\alpha = (r' - H\alpha)_{\text{obs}} - (r' - H\alpha)_{\text{fit}} \quad (1)$$

where  $(r' - H\alpha)_{\text{obs}}$  is the observed value of the colour and  $(r' - H\alpha)_{\text{fit}}$  is the value obtained from the fit for the corresponding observed value of  $r' - i'$ . The selection criterion is then given in terms of H $\alpha$  excess by

$$\Delta H\alpha > C \sqrt{[rms^2 + \sigma_{(r'-H\alpha)}^2] + m_{\text{fit}}^2 \sigma_{(r'-i')}^2}. \quad (2)$$

Here  $rms$  is the root mean square value of the residuals around the fit,  $C$  is a constant (we use values of 4.5 for our initial fits and 5 for the fits with  $\sigma$ -clipping),  $m_{\text{fit}}$  is the gradient of the fit line, and  $\sigma_{(r'-H\alpha)}$  and  $\sigma_{(r'-i')}$  are the errors on the observed colours.

Note that the cut lines shown here are only approximate, as the actual selection criterion used also considers the errors on each individual datapoint (see Equation 2).

In the example shown in Fig. 1, the lines illustrate the initial and final selection cuts applied. However the cut lines shown are only approximate, as the actual selection criterion used also considers the errors on each individual datapoint (see Equation 2) and this is not reflected by the cut lines shown in the figure. This explains why in some cases objects appearing above the illustrated cuts are not selected as emitters. The selected H $\alpha$  emitters are indicated by the large triangles. The figure shows data from IPHAS field 5455, which contains the CV EY Cyg. Note that the data quality of this field falls below the IPHAS standards, that is this field will be re-observed for the final IPHAS survey at a latter date. EY Cyg is a bright dwarf nova with V-band magnitudes of 11.4 and 15.5 in outburst and quiescence, respectively. The IPHAS photometry ( $r' = 14.1$ ) suggests the system was observed near quiescence, when it is known to display clear H $\alpha$  emission (Munari et al. 1997). The CV is marked by a large open circle and was correctly selected as a likely emission line object by our algorithm. We note that, in this case, the final fit succeeded in identifying EY Cyg as an emission line object, whereas a selection based on the initial fit to all the data would have failed to do so.

It is worth emphasizing that we make no claim that the method presented here is in any strict sense optimal for selecting H $\alpha$  emitters. The design goals for our algorithm are merely that it should be simple, fully automated and produce reasonable results in the vast majority of cases (when compared to a fully interactive outlier selection). Consequently, the selection criteria we use are essentially empirical and tailored to provide adequate results in most situations.

**Table 1.** Summary of the existing data for the CVs in the two samples. Magnitude ranges are drawn directly from the Downes *et al* catalogue. Orbital period information is drawn directly from the Ritter and Kolb catalogue. CV classification data are adapted from the information contained within CVCat.

GCVS Name	Other name	Magnitude Range	Orbital Period <sup>a</sup> (days)	CV Flag <sup>b</sup>	CV Type <sup>c</sup>
<b>Off-Plane</b>					
RZ LMi	PG 0948+344	14.2 V - 16.8 V	0.058500*	0	DN/SU
RU LMi	CBS-119/Ton 1143	13.8 p - 19.5 p	0.251000	0	DN
CH UMa	PG 1003+678	10.7 V - 15.3 V	0.343184	0	DN
SW Sex	PG 1012-029	14.8 B - 16.7 B	0.134938	0	NL/SW
GG Leo	RX J1015.5+0904	16.5 V - 18.8 V	0.055471	0	AM
CP Dra		14.3 p - 20 p	0.081600*	0	DN
CI UMa	SVS 1755	13.8 p - 18.8 V	0.060000	0	DN/SU
KS UMa	RX J1020+5304	13.0 p - 17.0 p	0.068000	0	DN
FIRST J102347+003841		17.3 V - 17.8 V	0.198115	-1	-
U Leo	BD +14 2239	10.5 v - <15 v	0.267400:	0	N:
DW UMa	PG 1030+590	14.9 V - 18. V	0.136607	0	NL/VY
DO Leo	PG 1038+155	16.0 B - 17.0 B	0.234515	0	NL
IY UMa	Tmz V85	13.0 p - 18.4 p	0.073909	0	DN/SU
CW 1045+525		16.5 B -	0.271278	0	DN
SX LMi	CBS-31/Ton 45	13 V - 17.4 V	0.067200	0	DN/SU
CY UMa	SVS 2198	12.3 V - 17.8 V	0.067950	0	DN/SU
AN UMa	PG 1101+453	13.8 B - 20.2 B	0.079753	0	AM
ST LMi	CW 1103+254	15.0 V - 17.2 V	0.079089	0	AM
AR UMa	1ES 1113+432	13.3 V - 16.5 V	0.080501	0	AM
DP Leo	1E 1114+182	17.5 B - 19.5 B	0.062363	0	AM
TT Crt	FSV 1132-11	12.7 V - 16.3 V	0.268420	0	DN
RZ Leo		11.5 V - 19.2 V	0.076038	0	DN/SU
T Leo	BD +4 2506a	10.0 V - 15.9 V	0.058820	0	DN/SU
DO Dra	YY Dra?	10.6 B - 16.7 B	0.165374	0	IP
TW Vir	PG 1142-041	12.1 v - 16.3 v	0.182670	0	DN
EU UMa	RE 1149+28	16.5 B - 16.8 B	0.062600	0	AM
BC UMa	GR 102	10.9 B - 18.3 B	0.062610	0	DN/SU
IR Com	S 10932	13.5 B - 18. B	0.087039	0	DN:/SU:
EV UMa	RX J1307+53	17.1 V - 20.8 V	0.055338	0	AM
HV Vir	NSV 6201	11.5 V - 19.0 V	0.057069	0	DN/SU
HS Vir	PG 1341-079	13.0 B - 16.6 V	0.076900	0	DN
OU Vir	1432-0033	14.5 p - 18.5 j	0.072730	0	DN/SU
UZ Boo	HV 10426	11.5 v - 20.4 V	0.125000:	0	DN/SU
KV Dra	RX J1450.5+6403	11.8 V - 17.1 V	0.058760	0	DN/SU
TT Boo	HV 3681	12.7 v - 19.2 V	0.077000:	0	DN/SU
NY Ser	NSV 6990	14.8 V - 17.9 V	0.097800	0	DN/SU
M5 V101		17.5 p - 20.9 V	0.242000	0	DN
ES Dra	PG 1524+622	13.9 p - 16.3 p	0.179000	0	DN/SU
QW Ser	Tmz V46	12.8 p - <15.3 p	0.074570	0	DN
ASAS 153616-0839.1		11.5 V - <15.4 V	0.063600*	0	DN
LX Ser	Stepanian's star	13.3 B - 17.4 B	0.158432	0	NL/SW
CT Ser	N Ser 1948 (r)	7.9 v - 16.6 p	0.195000	0	N
SS UMi	PG 1551+719	12.6 V - 17.6 V	0.067780	0	DN/SU
MR Ser	PG 1550+191	14.9 V - 17. V	0.078798	0	AM

<sup>a</sup> A colon following the orbital period signifies the value is uncertain, an asterisk signifies the value has been estimated from the known superhump period.<sup>b</sup> Possible entries in this column; 0 = good, 1= uncertain, -1 = not in CV Cat, -2 = non cv.<sup>c</sup> Possible entries in this column; DN = dwarf nova, N = nova, NL = novalike variable, NR = recurrent nova, AM = polar (AM Her), IP = intermediate polar, - = non classified. Any entries in this column following a forward slash are the secondary classification of the CV, possible additional entries are; SU = SU UMa system, VY = VY Scl system, ZC = Z Cam system, UG = U Gem system, SW = SW Sex system, Na = fast nova, Nb = slow nova. A colon following any of these entries signifies the classification is uncertain.

Table 1 – continued

GCVS Name	Other name	Magnitude Range	Orbital Period <sup>a</sup> (days)	CV Flag <sup>b</sup>	CV Type <sup>c</sup>
<b>Off-Plane</b>					
RX J1554.2+2721		16.8 B -	0.105462	0	AM
QZ Ser	HadV4	12.7 p - <14.9 p	0.083161	0	DN
VW CrB	Antipin V21	14.0 p - <17.5 b	0.070700*	0	DN
1RXS J161008+035222			0.132200	0	AM
X Ser	HV 3137	8.9 p - 18.3 p	1.480000	0	N:/Nb:
V589 Her	S 10296	14.1 p - <17.5 p	0.090500*	0	DN
V844 Her	Antipin V43	12.5 p - 17.5 p	0.054643	0	DN/SU
V699 Oph	HV 10577	13.8 p - 18.5 p	0.068300*	-2	-
RW UMi	SVS 1359	6 p - 18.5 B	0.059100	0	N/Nb
V841 Oph	BD -12 4633	4.2 v - 13.5 v	0.601400	0	N/Nb
<b>Plane</b>					
HT Cas	S 3343	10.8 v - 18.4 v	0.073647	0	DN/SU
V Per	BD +56 406a	9.2 p - 18.5 p	0.107126	0	N
UV Per	AN 87.1911	11.7 V - 17.9 V	0.064900	0	DN/SU
TZ Per	AN 28.1912	12.3 v - 15.6 v	0.262906	0	DN/ZC
T Aur	BD +30 923a	4.2 p - 15.2 p	0.204378	0	N/Nb
FS Aur	S 3946	14.4 v - 16.2 v	0.059500	0	DN
CW Mon	AN 61.1936	11.9 v - 16.3 v	0.176600	0	DN
V603 Aql	HD 174107	-1.1 v - 11.8 B	0.138500	0	N/Na
CI Aql	AN 23.1925	8.8 V - 15.6 p	0.618363	0	NR
V446 Her		3.0 p - 17.8 B	0.207000	0	N/Na
V1425 Aql		7.5 v - <19.0 V	0.255800	0	N/IP:
EM Cyg	AN 185.1928	12.5 v - 14.4 v	0.290909	0	DN/ZC
RX J1951.7+3716		15.5 B -	0.493000	0	-
EY Cyg	AN 200.1928	11.4 v - 15.5 v	0.459326	0	DN/UG
V2306 Cyg	1WGA J1958.2+3232	15.7 V -	0.181200	0	IP
V550 Cyg	S 3847	14.2 p - <17.0 p	0.067200*	0	DN/UG
V503 Cyg	S 4524	13.4 V - 17.6 V	0.077700	0	DN/SU
V751 Cyg	SVS 1202	13.2 V - 16.0 V	0.144464	0	NL/VY
V2275 Cyg	N Cyg 2001, No. 2	6.6 p -	0.314500	0	N

<sup>a</sup> A colon following the orbital period signifies the value is uncertain, an asterisk signifies the value has been estimated from the known superhump period.

<sup>b</sup> Possible entries in this column; 0 = good, 1 = uncertain, -1 = not in CV Cat, -2 = non cv.

<sup>c</sup> Possible entries in this column; DN = dwarf nova, N = nova, NL = novalike variable, NR = recurrent nova, AM = polar (AM Her), IP = intermediate polar, - = non classified. Any entries in this column following a forward slash are the secondary classification of the CV, possible additional entries are; SU = SU UMa system, VY = VY Scl system, ZC = Z Cam system, UG = U Gem system, SW = SW Sex system, Na = fast nova, Nb = slow nova. A colon following any of these entries signifies the classification is uncertain.

Table 2: Summary of the IPHAS data for the CVs in the two samples.

GCVS Name	Other name	RA	DEC	$\ell$	$b$	$r'$	$r'$	$i'$	$i'$	$H\alpha$	$H\alpha$	Emitter <sup>a</sup>	Initial <sup>b</sup>	Field <sup>c</sup>	$i'$ band	$i'$ band	$i'$ band	EW <sup>d</sup>	
		(2000)	(2000)	( $^{\circ}$ )	( $^{\circ}$ )		error		error				Selection	Quality	$i'$ band	$i'$ band	$i'$ band	( $\text{\AA}$ )	
													Flag	Flag	(arcsec)	Ellipticity	Magnitude	Limit	
<b>Off-Plane</b>																			
RZ LMi	PG 0948+344	09:51:48.93	+34:07:23.9	191.29	51.04	14.789	0.001	14.783	0.003	14.857	0.003	0	0	0	1.83	0.09	20.03	-5	
RU LMi	CBS-119/Ton 1143	10:02:07.47	+33:51:00.5	191.83	53.17	17.626	0.006	17.296	0.013	17.007	0.008	1	0	0	1.42	0.10	20.47	65	
CH UMa	PG 1003+678	10:07:00.59	+67:32:47.2	142.90	42.65	14.327	0.001	13.683	0.002	13.832	0.002	1	0	1	2.29	0.04	20.00	35	
SW Sex	PG 1012-029	10:15:09.39	-03:08:32.9	245.52	41.68	15.071	0.002	14.952	0.004	14.815	0.003	1	0	1	2.53	0.10	19.62	25	
GG Leo	RX J1015.5+0904	10:15:34.67	+09:04:42.5	231.59	49.05	18.949	0.014	18.936	0.047	19.122	0.032	0	0	1	1.65	0.07	20.20	-15	
CP Dra		10:15:39.82	+73:26:05.2	136.34	39.38	15.587	0.002	15.628	0.005	15.796	0.004	0	0	0	1.44	0.07	20.58	-15	
CI UMa	SVS 1755	10:18:12.96	+71:55:43.6	137.59	40.55	18.490	0.010	18.247	0.023	18.036	0.014	1	0	0	1.20	0.12	20.80	45	
KS UMa	RX J1020+5304	10:20:26.52	+53:04:33.2	159.55	51.93	16.775	0.004	16.539	0.008	15.953	0.004	1	0	0	0.75	0.09	20.86	110	
FIRST J102347+003841		10:23:47.70	+00:38:41.2	243.49	45.78	17.315	0.005	16.856	0.010	17.315	0.009	0	0	1	1.83	0.07	20.41	-10	
U Leo	BD +14 2239	10:24:03.92	+14:00:25.3	226.34	53.27	17.007	0.004	16.696	0.009	17.063	0.008	0	0	0	1.08	0.10	20.53	-10	
DW UMa	PG 1030+590	10:33:52.86	+58:46:54.8	150.28	50.41	15.211	0.002	15.116	0.004	14.421	0.002	1	0	0	0.70	0.07	20.85	110	
DO Leo	PG 1038+155	10:40:51.23	+15:11:34.0	227.71	57.43	17.591	0.006	16.947	0.010	17.136	0.009	1	0	0	1.32	0.04	20.64	30	
IY UMa	Tmz V85	10:43:56.72	+58:07:31.9	149.76	51.84	17.638	0.006	17.299	0.012	17.046	0.008	0	2	1	2.31	0.12	20.11	65	
CW 1045+525		10:48:18.01	+52:18:30.0	156.89	55.92	14.608	0.001	14.000	0.002	14.164	0.002	1	0	0	1.50	0.04	20.63	30	
SX LMi	CBS-31/Ton 45	10:54:30.44	+30:06:10.4	199.34	64.24	16.146	0.003	15.917	0.006	15.596	0.004	1	0	0	1.36	0.05	20.42	60	
CY UMa	SVS 2198	10:56:57.03	+49:41:18.3	159.37	58.55	17.336	0.005	16.995	0.011	16.534	0.006	1	0	0	1.39	0.05	20.42	100	
AN UMa	PG 1101+453	11:04:25.62	+45:03:14.5	165.83	62.15	16.251	0.003	16.103	0.006	15.908	0.004	1	0	1	1.97	0.05	20.33	35	
ST LMi	CW 1103+254	11:05:39.79	+25:06:28.7	211.80	66.21	17.523	0.005	16.681	0.009	17.343	0.010	0	0	0	1.30	0.07	20.49	-5	
AR UMa	1ES 1113+432	11:15:44.56	+42:58:22.6	167.45	64.97	16.468	0.003	15.962	0.006	16.269	0.005	0	0	0	0.75	0.06	20.77	5	
DP Leo	1E 1114+182	11:17:15.93	+17:57:41.8	230.90	66.46	18.082	0.007	17.915	0.018	17.723	0.012	1	0	1	2.06	0.02	20.11	35	
TT CrI	FSV 1132-11	11:34:47.17	-11:45:30.2	274.88	46.90	15.729	0.002	15.156	0.004	15.379	0.003	1	0	1	2.78	0.11	19.48	20	
RZ Leo		11:37:22.24	+01:48:58.9	264.77	59.09	18.715	0.011	18.013	0.020	17.932	0.014	1	0	1	2.47	0.03	19.77	80	
T Leo	BD +4 2506a	11:38:26.81	+03:22:07.5	263.49	60.52	16.048	0.002	15.676	0.005	14.993	0.003	1	0	1	2.69	0.20	19.42	155	
DO Dra	YY Dra?	11:43:38.46	+71:41:20.9	130.30	44.46	14.516	0.001	13.872	0.002	13.485	0.001	1	0	0	1.37	0.07	20.53	130	
TW Vir	PG 1142-041	11:45:21.18	-04:26:05.7	273.60	54.63	15.763	0.002	15.199	0.004	15.112	0.003	1	0	0	1.74	0.05	20.33	60	
EU UMa	RE 1149+28	11:49:55.71	+28:45:07.5	202.54	76.33	17.283	0.004	17.140	0.011	16.477	0.006	1	0	1	2.49	0.05	19.87	110	
BC UMa	GR 102	11:52:15.84	+49:14:41.9	146.27	65.12	18.157	0.007	17.971	0.019	17.570	0.011	1	0	1	2.04	0.11	20.01	70	
IR Com	S 10932	12:39:32.05	+21:08:06.3	277.93	83.42	18.618	0.010	17.809	0.018	18.534	0.020	0	0	0	1.08	0.04	20.55	-10	
EV UMa	RX J1307+53	13:07:53.82	+53:51:31.0	117.57	63.10	16.630	0.003	16.759	0.009	16.495	0.006	1	0	0	1.07	0.06	20.65	20	
HV Vir	NSV 6201	13:21:03.18	+01:53:29.0	319.88	63.78	19.058	0.014	19.013	0.040	18.938	0.025	0	2	0	1.18	0.07	20.74	10	
HS Vir	PG 1341-079	13:43:38.44	-08:14:03.6	324.44	52.44	15.206	0.002	14.980	0.003	14.839	0.003	1	0	0	1.17	0.12	20.74	35	
OU Vir	1432-0033	14:35:00.23	-00:46:06.2	348.90	52.60	16.556	0.003	16.445	0.007	16.013	0.005	1	0	1	1.84	0.06	20.11	65	
KV Dra	RX J1450.5+6403	14:50:38.34	+64:03:28.8	103.81	48.41	17.086	0.004	16.766	0.009	16.439	0.006	1	0	0	1.80	0.03	20.25	70	
TT Boo	HV 3681	14:57:44.79	+40:43:40.9	68.74	60.70	13.688	0.001	13.722	0.002	13.740	0.002	0	2	0	0.74	0.07	20.99	-5	
NY Ser	NSV 6990	15:13:02.33	+23:15:08.5	33.99	57.84	15.311	0.002	15.269	0.004	15.341	0.003	0	0	0	0.82	0.04	20.82	-5	
ES Dra	PG 1524+622	15:25:31.80	+62:00:59.8	97.64	46.83	15.019	0.001	14.823	0.003	14.905	0.003	1	0	0	0.89	0.17	20.72	5	
QW Ser	Tmz V46	15:26:13.99	+08:18:02.5	13.06	48.86	17.603	0.005	17.140	0.012	16.941	0.008	1	0	0	1.72	0.04	20.08	70	
ASAS 153616-0839.1		15:36:16.00	-08:39:07.7	356.94	36.40	18.096	0.007	17.852	0.018	16.993	0.008	1	0	0	0.80	0.11	20.76	175	
LX Ser	Stepanian's star	15:38:00.11	+18:52:03.5	29.78	50.97	14.762	0.001	14.431	0.003	14.162	0.002	1	0	0	0.70	0.06	21.02	65	
CT Ser	N Ser 1948 (r)	15:45:39.09	+14:22:31.5	24.48	47.56	16.434	0.003	16.351	0.007	16.360	0.006	1	0	0	0.83	0.04	20.96	5	
SS UMi	PG 1551+719	15:51:22.37	+71:45:12.1	106.37	39.06	16.001	0.002	15.901	0.006	15.741	0.004	1	0	0	0.61	0.14	20.72	25	
MR Ser	PG 1550+191	15:52:47.16	+18:56:29.2	31.72	47.71	17.129	0.004	16.468	0.008	17.003	0.008	0	0	1	1.65	0.04	20.39	-5	
RX J1554.2+2721		15:54:12.35	+27:21:52.7	44.16	49.61	17.103	0.004	16.243	0.007	16.418	0.006	1	0	1	1.66	0.08	20.21	55	
QZ Ser	HadV4	15:56:54.56	+21:07:19.9	35.24	47.49	17.192	0.004	16.576	0.008	16.731	0.007	1	0	0	1.74	0.05	20.17	35	
VW CrB	Antipin V21	16:00:03.71	+33:11:14.2	53.29	49.12	16.652	0.003	16.392	0.007	16.633	0.006	0	0	0	0.74	0.06	20.85	-5	
1RXS J161008+035222		16:10:07.55	+03:52:33.1	15.81	37.26	17.596	0.005	16.262	0.007	16.899	0.007	1	0	0	1.03	0.05	20.74	40	
X Ser	HV 3137	16:19:17.70	-02:29:29.3	10.84	31.87	17.050	0.004	16.544	0.008	16.648	0.006	1	0	0	0.93	0.09	20.62	30	
V589 Her	S 10296	16:22:07.19	+19:22:36.8	35.56	41.33	17.610	0.006	17.127	0.011	16.899	0.008	1	0	1	2.13	0.03	19.98	75	
V844 Her	Antipin V43	16:25:01.76	+39:09:26.6	62.36	44.38	17.656	0.005	17.486	0.014	16.730	0.007	1	0	0	0.66	0.06	20.82	135	
V699 Oph	HV 10577	16:25:14.79	-04:40:25.7	9.73	29.41	15.915	0.002	15.173	0.004	15.699	0.004	0	0	0	0.82	0.08	20.78	0	
RW UMi	SVS 1359	16:47:54.84	+77:02:12.2	109.64	33.15	18.677	0.010	18.531	0.031	18.454	0.018	1	0	0	0.74	0.15	20.76	20	
V841 Oph	BD -12 4633	16:59:30.38	-12:53:26.8	7.62	17.78	13.344	0.001	12.937	0.001	13.203	0.001	0	2	0	1.09	0.07	20.53	5	

**Plane**

Continued on Next Page...

Table 2 – Continued

GCVS Name	Other name	RA	DEC	$\ell$	$b$	$r'$	$r'$	$i'$	$i'$	$H\alpha$	$H\alpha$	Emitter <sup>a</sup>	Initial <sup>b</sup>	Field <sup>c</sup>	$i'$ band	$i'$ band	$i'$ band	EW <sup>d</sup> (Å)
		(2000)	(2000)	(°)	(°)	error	error	error	error	Selection Flag	Quality Flag		Seeing (arcsec)	Ellipticity	Magnitude Limit			
HT Cas	S 3343	01:10:13.17	+60:04:35.6	125.27	-2.71	15.936	0.004	15.455	0.005	15.056	0.003	1	0	0	1.24	0.06	20.06	110
V Per	BD +56 406a	02:01:53.93	+56:44:03.5	132.52	-4.82	17.983	0.014	17.746	0.018	17.378	0.011	1	0	0	0.85	0.06	20.55	70
UV Per	AN 87.1911	02:10:08.30	+57:11:21.0	133.47	-4.06	18.195	0.015	17.763	0.018	17.110	0.009	1	0	0	0.85	0.06	20.67	160
TZ Per	AN 28.1912	02:13:50.95	+58:22:52.4	133.58	-2.78	12.673	0.001	12.465	0.001	12.586	0.001	0	0	0	1.02	0.08	20.51	5
T Aur	BD +30 923a	05:31:59.12	+30:26:45.4	177.14	-1.70	14.910	0.003	14.573	0.003	14.603	0.003	1	0	0	1.25	0.04	20.38	25
FS Aur	S 3946	05:47:48.37	+28:35:11.2	180.55	0.23	15.797	0.004	15.350	0.004	15.241	0.004	1	0	0	0.99	0.10	20.52	55
CW Mon	AN 61.1936	06:36:54.59	+00:02:17.3	211.24	-3.21	18.339	0.094	17.094	0.049	17.180	0.039	0	0	1	1.17	0.05	18.45	130
V603 Aql	HD 174107	18:48:54.64	+00:35:03.0	33.16	0.83	12.425	0.001	11.995	0.001	11.835	0.001	0	2	0	0.88	0.08	20.67	60
CI Aql	AN 23.1925	18:52:03.57	-01:28:39.0	31.69	-0.81	15.562	0.002	14.812	0.003	15.438	0.004	0	0	0	1.08	0.07	20.54	-5
V446 Her		18:57:21.61	+13:14:29.7	45.41	4.71	16.759	0.005	16.242	0.008	16.443	0.007	1	0	0	1.47	0.08	19.73	20
V1425 Aql		19:05:26.66	-01:42:03.3	33.01	-3.89	18.494	0.011	18.693	0.042	15.731	0.004	0	2	0	1.30	0.10	20.29	456955 <sup>e</sup>
EM Cyg	AN 185.1928	19:38:40.13	+30:30:28.6	65.19	4.28	13.129	0.001	12.697	0.001	12.881	0.001	1	0	0	1.84	0.09	19.57	15
RX J1951.7+3716		19:51:47.50	+37:16:48.1	72.44	5.27	14.961	0.002	14.393	0.003	14.353	0.003	1	0	1	1.77	0.07	18.91	55
EY Cyg	AN 200.1928	19:54:36.77	+32:21:55.5	68.50	2.26	14.125	0.001	13.760	0.002	13.878	0.002	1	0	1	1.48	0.05	19.19	15
V2306 Cyg	1WGA J1958.2+3232	19:58:14.47	+32:32:42.2	69.05	1.70	15.479	0.002	15.240	0.004	15.092	0.003	1	0	0	0.91	0.06	20.38	35
V550 Cyg	S 3847	20:05:04.95	+32:21:22.9	69.66	0.38	16.621	0.003	15.922	0.006	16.544	0.006	0	0	0	1.12	0.07	20.63	-10
V503 Cyg	S 4524	20:27:17.39	+43:41:22.5	81.50	3.07	17.252	0.013	16.842	0.014	16.404	0.011	1	0	0	1.01	0.07	19.82	105
V751 Cyg	SVS 1202	20:52:12.80	+44:19:26.2	84.74	-0.09	13.879	0.002	13.653	0.002	13.712	0.002	0	0	0	1.00	0.06	20.59	10
V2275 Cyg	N Cyg 2001, No. 2	21:03:01.98	+48:45:53.5	89.32	1.39	17.709	0.011	17.017	0.011	17.312	0.010	1	0	1	3.04	0.08	19.24	25

<sup>1</sup> Possible entries in this column; 0 = not detected as a H $\alpha$  emitter, 1 = detected as a H $\alpha$  emitter

<sup>2</sup> Possible entries in this column; 0 = no flag, 2 = incorrect object classification or object too bright, 3 = magnitudes missing, 5 = situated on bad pixels

<sup>3</sup> Possible entries in this column; 0 = no flag, 1 = bad quality field that is, seeing > 2 or ellipticity < 0.2 or limiting magnitude < 19.5 in any of the three bands

<sup>4</sup> Values are estimates obtained from IPHAS photometry.

<sup>5</sup> This value is too large to be physically real.

#### 4.5 Interpreting H $\alpha$ Excess and Estimating Equivalent Widths

It is tempting to treat the H $\alpha$  excess values calculated from Equation 1 as direct tracers of emission line strength (tracers of line EW). However, this interpretation is not always safe. In particular, it is important to keep in mind that the calculated excess values have no fixed reference point, that is each excess is calculated relative to the local fit to the upper boundary of the stellar locus in the appropriate magnitude bin of a given field. Thus any direct comparison of H $\alpha$  excess values between different objects implicitly assumes that each object actually belonged to the stellar population that was described by the fit. In fields containing a split stellar locus (and hence more than one population), there is no guarantee that this is the case.

It is worth stressing that this problem is not simply due to the particular definition of ‘‘H $\alpha$  excess’’ we have adopted. Instead, it reflects the inherent ambiguity in assigning individual objects to particular stellar populations on the basis of limited photometric information. More specifically, since different stellar populations can have different ‘‘baseline’’ ( $r' - \text{H}\alpha$ ) colours at given ( $r' - i'$ ), it is impossible to define a physically meaningful H $\alpha$  *excess* for a given source without specifying the population to which it belongs.

This all sounds rather pessimistic. However, we can also turn this argument around: *if we are willing to adopt a particular spectral energy distribution (SED) for a given H $\alpha$  excess source, a corresponding H $\alpha$  EW estimate can be obtained immediately from the photometric data.* If this SED represents the objects’ continuum distribution better than the fit to the upper stellar locus, the resulting EW estimate should be a more meaningful quantity than the straight H $\alpha$  excess.

Fig. 2 illustrates how this idea can be implemented for CVs. Basically, the location of a given source in the colour-colour diagram is determined by its H $\alpha$  EW and the shape of its continuum SED. The latter, in turn, depends on the intrinsic SED shape and the reddening towards the source. For CVs, it may be reasonable to adopt an intrinsic SED of  $F_\lambda \propto \lambda^{-2.3}$  as typical. This is appropriate for an optically thick accretion disc and is probably acceptable even for WD-dominated short-period DNe. We can then add H $\alpha$  lines of varying EWs to this SED and calculate the reddening tracks of the resulting model spectra through colour-colour space. As shown in Fig. 2, this procedure yields a mapping between the observed colours, on the one hand, and the corresponding  $E_{B-V}$  values and H $\alpha$  EWs, on the other.

In principle, it should be possible to place observed points directly onto this mapped colour-colour plot and read off the resulting  $E_{B-V}$  values and H $\alpha$  EWs. However, in practice, one additional correction is necessary at present. This arises because our synthetic photometry is Vega-based, but the standard stars used for the photometric calibration of the IPHAS data are mostly later type stars. As noted by Drew et al. (2005), Vega is an A0V star with deep H $\alpha$  absorption, and this causes a systematic offset between observed and synthetic  $r' - \text{H}\alpha$  colours. The offset required for a given field is between 0.25 and -0.05 mag (in the sense that the data points must be shifted upwards). We thus account for this by applying an average shift of 0.15 mag to

**Table 3.** The distribution of H $\alpha$  emitters amongst the CV samples. The numbers are given as a ratio of CVs selected as H $\alpha$  emitters to the total number of CVs in the sample. The numbers in parenthesis show the corresponding percentages.

Sample	All CVs	CVs Passing initial cut
Off-Plane	36/52 (69.2)	36/48 (75.0)
In-Plane	12/19 (63.2)	12/17 (70.6)
Total	48/71 (67.6)	48/65 (73.8)

the observed  $r' - \text{H}\alpha$  colours of all CVs before placing them on Fig. 2.

It is also worth noting that the IPHAS data currently still lack a global (field-to-field) photometric calibration. This again particularly affects the H $\alpha$  photometry and causes a scatter of  $\approx 0.1$  mag in the  $r' - \text{H}\alpha$  colours between different fields. We currently make no attempt to correct for this. Note that both systematic and field-to-field offsets will be automatically corrected in the final IPHAS data release.

Fig. 2 shows the corrected colours of our CVs on the mapped colour-colour diagram. The resulting H $\alpha$  EW estimates are given in Table 2, and we will adopt these values throughout the rest of this paper. We stress that these may be subject to considerable error, both because of field-to-field scatter and because the intrinsic SED shape we have assumed may not be appropriate to all systems.<sup>4</sup>

## 5 RESULTS

Table 1 summarizes the key properties of all the CVs in the two samples. The magnitude range data were taken from the Downes *et al* catalogue<sup>5</sup> (Downes et al. 2001), orbital periods are from the Ritter & Kolb catalogue, and the CV type information comes from the web-based CV catalogue CVCat<sup>6</sup> (Kube et al. 2003). Our new data are listed Table 2, which also includes information on whether a given CV was selected as an H $\alpha$  emitter.

### 5.1 Recovery Rates of CVs as H $\alpha$ Emitters

Our recovery rates are summarized in Tables 3-6 and illustrated in Figs 3-4. In the following subsections, we discuss the resulting completeness estimates and their dependence on key CV properties (orbital period, CV type, apparent magnitude, galactic latitude). We also explore the causes that prevent some CVs from being selected as H $\alpha$  emitters.

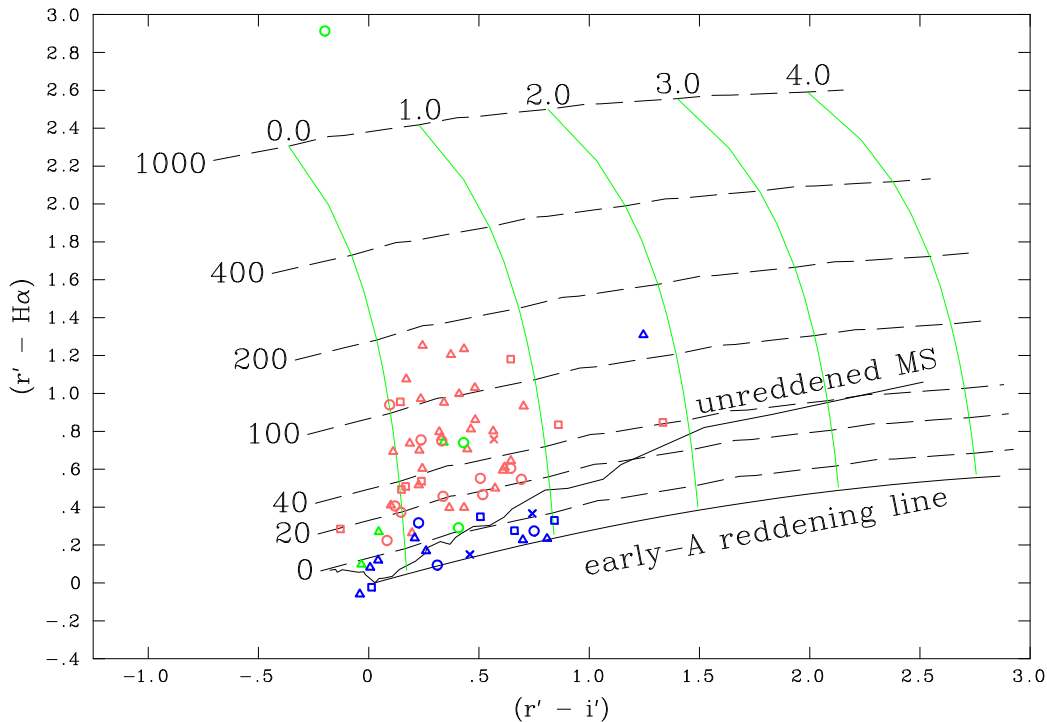
#### 5.1.1 Overall Completeness

Table 3 gives the recovery rates (that is CVs selected as H $\alpha$  emitters) for both in-plane and off-plane samples and also the combined recovery rates. We find a global recovery

<sup>4</sup> On a more positive note, Figure 6 in Drew et al. (2005) shows that, for *smooth* SEDs, most of the sensitivity to the assumed SED shape is in the reddening estimates, whereas H $\alpha$  EWs are much less affected.

<sup>5</sup> <http://archive.stsci.edu/prepds/cvcat/index.html>

<sup>6</sup> <http://cvcat.net>



**Figure 2.** Colour-colour plot showing how H $\alpha$  EW relates to H $\alpha$  excess and broad-band colour. Triangles represent dwarf novae; circles represent novae, novalike variables and recurrent novae; squares represent magnetic systems and crosses represent non-classified systems. The symbols are plotted in red if the system is a H $\alpha$  emitter; blue if it is a non-emitter; and green if it is a system which did not pass our initial selection cuts. The jagged solid curve is the unreddened main sequence (MS) line, the smooth solid curve running mainly horizontally is the early-A reddening line (that is the reddening track of an early A star). All other lines correspond to power law SEDs with  $F_\lambda \propto \lambda^{-2.3}$ , as appropriate for an optically thick accretion disc (see Drew et al. 2005). The dashed lines are lines of constant H $\alpha$  EW superposed on this SED (the EW values are given in Angstroms at the far left of each line). The solid green vertical lines represent H $\alpha$  emission curves of growth for this SED at fixed reddening (the corresponding E(B - V) values are shown at the top of each line).

rate of  $\simeq 68\%$  [48/71] for all CVs and  $\simeq 74\%$  [48/65] if we only consider those CVs that passed our initial selection cuts defined in section 4.1.

Both of these numbers are important. The first provides an “end-to-end” estimate of the survey completeness for CVs, that is what fraction of CVs brighter than  $r' = 19.5$  should we expect to discover with IPHAS (or similar surveys) as emission line objects. This estimate allows for incompleteness due to crowding/blending, objects falling on bad pixels, astrometric calibration problems, etc. By contrast, the second completeness estimate (considering only objects that pass our initial selection cuts) is an estimate of the fraction of CVs that are *in principle* discoverable by IPHAS, that is the fraction of CVs that exhibit photometrically detectable H $\alpha$  excesses. Note that the number of CVs detected as H $\alpha$  emitters is the same in both cases, since a CV which does not pass the initial selection cuts can never be selected as an H $\alpha$  emitter.

It is interesting to ask what constitutes a “detectable” H $\alpha$  excess in this context. A useful perspective on this question can be obtained from Fig. 2, which shows that the

unreddened main sequence broadly separates sources detected as H $\alpha$  emitters from sources not detected as H $\alpha$  excess objects. This reflects the fact that our selection procedure uses the upper boundary of the main stellar locus as the zero point in searching for “significant” H $\alpha$  excess outliers and confirms that this boundary usually tracks the unreddened main sequence.

It is worth noting that this effectively constitutes an observational selection bias. For a given SED, reddened sources must have larger H $\alpha$  EWs than unreddened sources in order to be selected as H $\alpha$  excess objects. Most CVs are blue objects observed through relatively little extinction, so the sense of this selection bias works in their favour. In essence, CVs occupy a region in the colour-colour plots where even a small H $\alpha$  EW stands out prominently from the stellar locus. The high recovery rate we find is partly due to this fortunate situation.

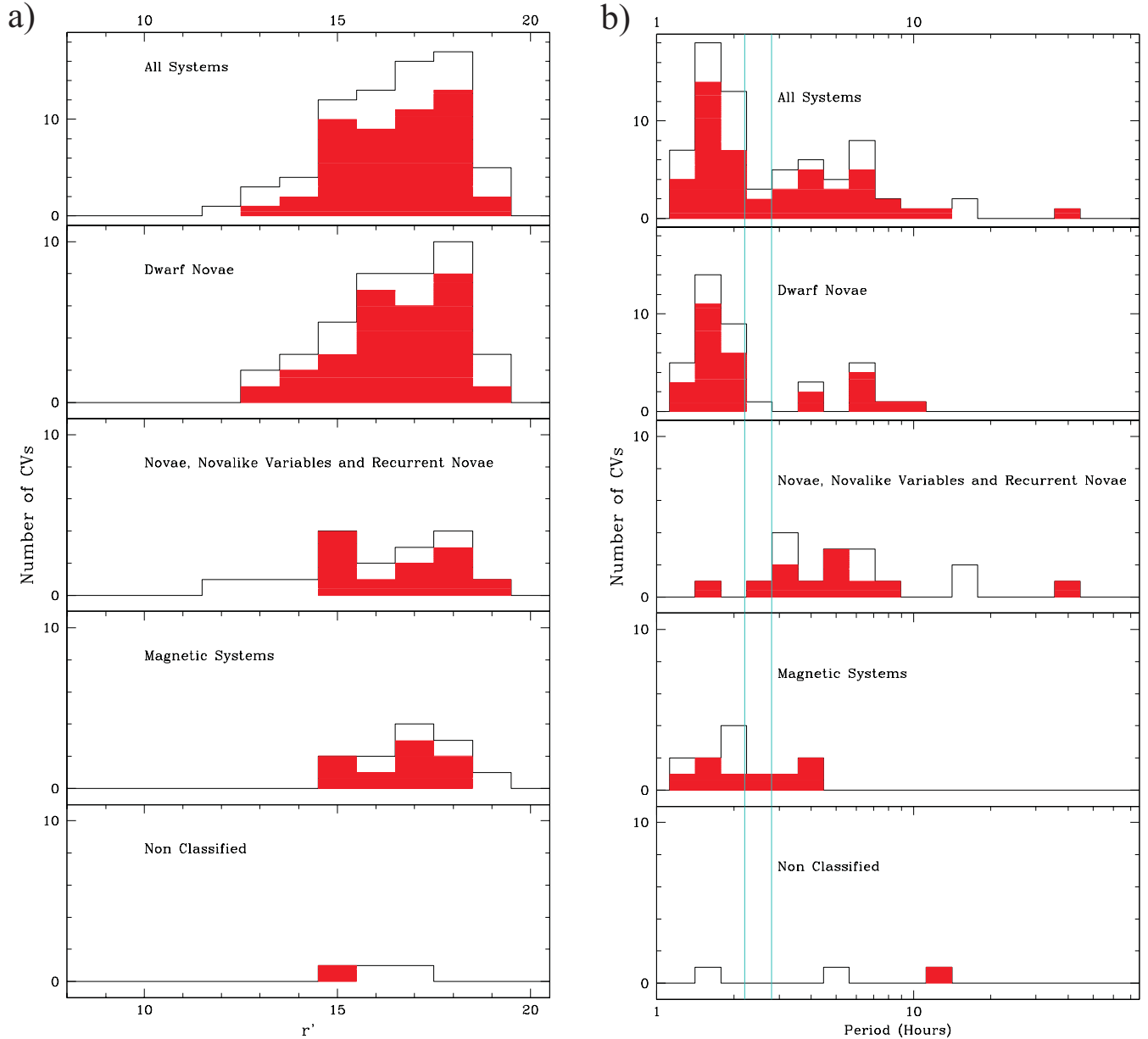


**Figure 3.** a) The magnitude distribution of the CVs b) the period distribution of the CVs. The orbital period gap is shown between the cyan lines. The plots show the distribution of emitters in red overlaid on top of the total distribution of CVs.

**Table 4.** A summary of the results showing the distribution amongst the long and short period CVs. Numbers are given as a ratio of CVs selected as  $H\alpha$  emitters to the total number of CVs in the sample, the percentages are given parenthesis.

	Sample	All CVs	CVs passing initial cut
Short Period < 2.5 hr	Off-Plane	21/34 (61.8)	21/31 (67.7)
	In-Plane	4/5 (80.0)	4/5 (80.0)
	Total	25/39 (64.1)	25/36 (69.4)
Long Period > 2.5 hr	Off-Plane	15/18 (83.3)	15/17 (88.2)
	In-Plane	8/14 (57.1)	8/12 (66.7)
	Total	23/32 (71.9)	23/29 (79.3)

### 5.1.2 Dependence on Orbital Period

In order to assess the dependence of our completeness on orbital period, we first compare the recovery statistics of short-period CVs (defined as having orbital periods below the 2.2 - 2.8 hour period gap) to those of long-period CVs (with periods above the gap). These recovery rates for both types of CVs are listed in Table 4.

Somewhat surprisingly, the recovery rates for long- and short-period systems are comparable, with both lying near 65 per cent. Given that short-period CVs tend to be intrinsically faint and that the  $H\beta$  EW and absolute magnitude for DNe are correlated (in the sense that the faint systems have stronger lines; Patterson 1984), one might have expected that short-period systems would be easier to detect and thus have higher recovery rates. The fact that we do

**Table 5.** Results showing the distribution of H $\alpha$  emitters amongst the two samples of CVs. The results in this case are separated by CV type. Numbers are given as a ratio of CVs selected as H $\alpha$  emitters to the total number of CVs in the sample, and the percentages are shown in parenthesis.

CV type	Sample	All CVs	CVs passing initial cut
Dwarf Novae	Off-Plane	22/30 (73.3)	22/27 (81.5)
	In-Plane	6/9 (66.7)	6/9 (66.7)
	Total	28/39 (71.8)	28/36 (77.8)
Magnetic Systems	Off-Plane	7/11 (63.6)	7/11 (63.6)
	In-Plane	1/1 (100.0)	1/1 (100.0)
	Total	8/12 (66.7)	8/12 (66.7)
Nova, Recurrent Nova and Novalike Variables	Off-Plane	7/9 (77.8)	7/8 (87.5)
	In-Plane	4/8 (50.0)	4/6 (66.7)
	Total	11/17 (64.7)	11/14 (78.6)
Non Classified	Off-Plane	0/2 (0.0)	0/2 (0.0)
	In-Plane	1/1 (100.0)	1/1 (100.0)
	Total	1/3 (33.3)	1/3 (33.3)

not observe a marked difference in recovery rates is mainly a testament to the high data quality of IPHAS, that is its ability to separate even long-period objects with relatively weak emission lines from the main stellar loci in any given field. This explanation is supported by the fact that short-period DNe *do* exhibit the largest H $\alpha$  EWs (see section 6.1 and particularly Fig. 5).

### 5.1.3 Dependence on CV Type

In order to examine whether H $\alpha$  selection favours particular CV sub-types, each system in our samples is assigned one of four basic types based on their classification in CV-Cat shown in Table 1: (i) dwarf novae; (ii) novae and nova-likes; (iii) magnetic CVs; (iv) unclassified systems. Note that the second class includes both classical and recurrent novae, and the third class includes both intermediate polars and the strongly magnetic polars. We refrain from using a finer classification scheme since this would result in classes with extremely small numbers. It should also be pointed out that some intermediate polars are known to undergo dwarf nova outbursts. For the purposes of the work presented here, any system which has been classified as a magnetic CV is put into this category, irrespective of any similarities with weakly-magnetic systems.

Table 5 shows the recovery statistics as a function of CV types and Fig. 3 shows how the recovery statistics depend on CV magnitude and orbital period for the different CV types. The dwarf novae have the overall highest recovery rate, which is not surprising since, in quiescence, the accretion discs in these systems are at least partially optically thin and are well known to produce strong emission lines (see Warner 1995 and references therein). The magnetic systems show the second highest recovery rate of all systems. This is probably due to strong Balmer emission from their accretion streams (Cropper 1990; Ferrario & Wickramasinghe 1993).

The novae and nova-likes have the lowest overall recovery rates, and it is tempting to attribute this to their known observational and physical characteristics. At first sight, this

**Table 6.** A summary of the results, in this case showing how the recovery rate of H $\alpha$  emitters varies between the four magnitude bins. The numbers are given as a ratio of CVs selected as H $\alpha$  emitters to the total number of CVs in the sample and the percentages are shown in parenthesis

Magnitude range ( $r'$ )	Sample	All CVs	CVs passing initial cut
< 16	Off-Plane	10/16 (62.5)	10/14 (71.4)
	In-Plane	7/11 (63.6)	7/10 (70.0)
	Total	17/27 (63.0)	17/24 (70.8)
16 - 17.5	Off-Plane	14/19 (73.7)	14/19 (73.7)
	In-Plane	2/3 (66.7)	2/3 (66.7)
	Total	16/22 (72.7)	16/22 (72.7)
17.5 - 18.5	Off-Plane	10/12 (83.3)	10/11 (90.9)
	In-Plane	3/5 (60.0)	3/4 (75.0)
	Total	13/17 (76.5)	13/15 (86.7)
18.5 - 19.5	Off-Plane	2/5 (40.0)	2/4 (50.0)
	In-Plane	0/0 (N.A.)	0/0 (N.A.)
	Total	2/5 (40.0)	2/4 (50.0)

seems reasonable: both types of high-state, weakly-magnetic CVs tend to exhibit only weak emission lines when viewed at moderate inclinations (for example Shara et al. 1986; Warner 1987; Dhillon 1996). This is probably because these systems contain optically thick discs that produce mainly absorption line spectra (although often emission reversals are observed in the cores of absorption line profiles).

However, a closer look at the statistics suggests that the true explanation for the low recovery rates for these systems is more prosaic. In the last column of Table 5, we show the recovery rates that result if we restrict attention to systems that have passed the initial selection cut. Here, the recovery fraction of novae and nova-likes is the highest. These numbers are completely consistent with the corresponding ones for DNe and magnetic systems. Thus the reason for the lower overall recovery statistics for novae and nova-likes is simply that relatively more of these systems are misclassified as non-stellar in the IPHAS data.

It is worth asking why, despite the physical arguments given above, the recovery rates for novae and nova-likes are comparable to those of DNe. This question has actually already been answered implicitly in section 5.1.2. There, we noted that short-period CVs (which are dominated by DNe) do exhibit larger H $\alpha$  excesses than long-period CVs (which contain most of the novae and nova-likes), but that IPHAS is sensitive enough to still identify the weaker H $\alpha$  emission often seen in the latter.

Finally, the non-classified systems show a comparatively low recovery rate in comparison to other systems. Given that there are only 3 non-classified CVs it is not prudent to draw any firm conclusions from the low recovery rate.

### 5.1.4 Dependence on CV Magnitude

As photometric scatter increases towards fainter magnitudes, completeness may be expected to decrease. Clearly, a faint CV will on average need to display a greater H $\alpha$  excess in order to be detected. Table 6 shows how the recovery rate

of H $\alpha$  emitters depends on the magnitudes bins used in the selection. It can be seen that for the Off-Plane sample the recovery rate actually increases slightly as we go to fainter bins until we get to the faintest bin, where it drops to 40 per cent (but note that there are only 5 sources in this bin). The In-Plane sample also hovers at a near constant 60 to 70 per cent for the three brighter bins, and for this sample the faintest bin contains no objects. We conclude that completeness for CVs in IPHAS remains steady and high up to at least  $r' \simeq 18.5$ . The small numbers of fainter CVs in our samples prevent us from constraining the drop in completeness beyond this point more precisely.

## 5.2 Reasons for CVs Not Being Selected as H $\alpha$ Emitters

There are several reasons that can prevent a CV from being selected as an H $\alpha$  emitter:

(i) The CV is not located significantly above the main stellar locus in the colour-colour plots. In some cases, this may be due to weakness or absence of an H $\alpha$  emission line (as seen in erupting dwarf novae and some nova-like variables). Furthermore, the equivalent width of the H $\alpha$  emission line can sometimes change significantly during the orbital cycle, so some CVs may have been observed at phases where the emission is weak. Finally, at fainter magnitudes, the signal-to-noise may simply become insufficient to separate a CV from the main stellar locus.

(ii) The CV is located below the locus in the colour-colour plots, that is the CV shows H $\alpha$  absorption. This may again point towards an erupting dwarf nova or a nova-like variable.

(iii) The fitting process failed, and the CV is not selected due to the resulting selection cut being inappropriate.

(iv) The CV does not pass the initial selection cuts defined in section 4.1

In the following sections, we look in more detail at the various CV sub-types and check if we can understand why particular CVs were not recovered as emission line objects.

### 5.2.1 Dwarf Novae

The DNe are the most numerous class and generally show some of the largest H $\alpha$  excesses. However, they also show the greatest range in H $\alpha$  excesses, although this can be at least partly attributed to observing some systems in quiescence and others in outburst. RZ LMi, CP Dra, TT Boo, NY Ser, and TZ Per are the DNe that have been observed in outburst. None of them have been detected as H $\alpha$  emitters. Of the 6 DNe remaining that were not selected as H $\alpha$  emitters, IY UMa has a large H $\alpha$  excess but does not pass the initial selection cuts, for the reasons given in section 3.1, and hence is not selected. CW Mon also has a large H $\alpha$  excess but is not selected as described in section 6.1. HV Vir misses our initial selection cuts and hence is not selected, however its EW shows that H $\alpha$  emission is present. This leaves 3 systems which are not recovered as H $\alpha$  emitters: IR Com, VW CrB and V550 Cyg. These systems pass our initial selection cuts and do not have a field quality flag associated with them. It is likely that variations in EW due to orbital phase can account for the absence of observable H $\alpha$  emission in these

systems, for example IR Com is known to be an eclipsing system and the IPHAS magnitudes are consistent with this system being observed in eclipse.

The recovery rate for all the DNe in quiescence is 81 per cent<sup>7</sup> which is 9 per cent higher than the recovery rate for all the DNe including those in outburst.

### 5.2.2 Magnetic CVs

There are rather few magnetic systems in our samples (including only one intermediate polar), but the majority show a detectable H $\alpha$  excess. Those which do not show emission are all AM Her systems observed in the low state (GG Leo, ST LMi, AR UMa, and MR Ser). A reduction in H $\alpha$  emission line strength is a known characteristic of low state magnetic CVs. It is possible that the H $\alpha$  emission is not strong enough to be detected above Zeeman absorption in these systems.

### 5.2.3 Novae, Recurrent Novae and Novalike Variables

Many of the bluest CVs of this class show a large H $\alpha$  excess indicating that the nova remnants are undergoing mass transfer. However, there is no simple link between detection of H $\alpha$  excess and time since eruption. For example, V Per and T Aur erupted in 1891 and 1887, respectively, and both have been detected as emitters. Conversely, the two oldest nova remnants – V841 Oph (1848) and U Leo (1855, though its nature as a nova is not certain) – have not been detected as H $\alpha$  excess objects.

There is one nova with a very high H $\alpha$  excess that did not pass the initial selection cut. This system is V1425 Aql. Spectroscopic observations have shown strong H $\alpha$  emission both before and after outburst (Kamath et al. 1997), which is consistent with the large excess we observe.

## 5.3 In-Plane vs Off-Plane CVs

Given that IPHAS is a galactic plane survey, but that the majority of the CVs analyzed here are Off-Plane sources, it is worth checking whether crowding and extinction affects the recovery rate in galactic plane fields. We have already provided separate recovery rates for both samples in Tables 3-6, but in Fig. 4 we now additionally present a visual comparison between the recovery statistics of In-Plane and Off-Plane samples.

In general, we find that the recovery rates of the two samples are similar. This suggests that crowding and extinction have at most a small effect on completeness. However, despite the similar recovery rates, there is nevertheless a clear difference in data between galactic plane fields and non-galactic plane fields. For example, when the value of the rms scatter about the initial least square fits to the stellar loci is compared between In-Plane and Off-Plane fields, the scatter is clearly larger for the former. This is mainly due to different populations seen at different distances through varying extinction in galactic plane fields (though probably

<sup>7</sup> The CVs HS Vir and OU Vir have been excluded from this recovery rate calculation as the photometry suggests they are in an intermediate state between quiescence and outburst.

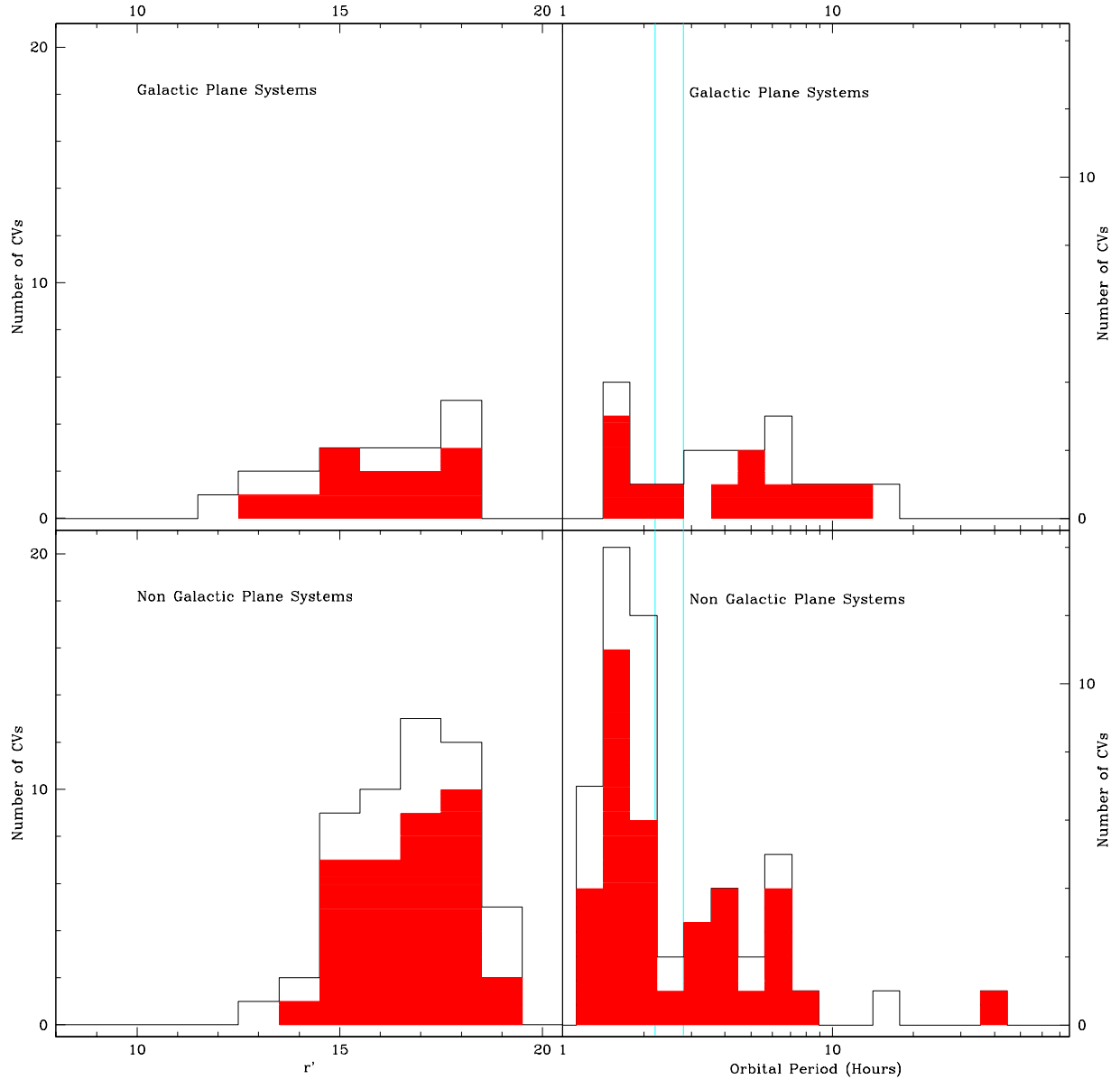


**Figure 4.** The magnitude distribution and period distribution of CVs showing those located within the galactic plane (upper plots) and outside of the plane (lower plots). The plots show the distribution of emitters in red overlaid on the total distribution of CVs. The orbital period gap is shown between the cyan lines.

also to increased photometric scatter due to higher crowding levels). Our  $\sigma$ -clipping fits to the upper boundary of the main stellar locus help partly to counter this effect. Without this technique, the In-Plane recovery rates would be reduced.

## 6 CORRELATIONS BETWEEN PHYSICAL AND PHOTOMETRIC PROPERTIES

### 6.1 Orbital Period vs $H\alpha$ EW

In Fig. 5, we plot the  $H\alpha$  EW – estimated as described in Section 4.5 – versus the orbital period for each CV. As explained in the introduction, short-period CVs are expected to show stronger  $H\alpha$  emission, and this is indeed confirmed by the figure.

The colour codes and plot symbols are defined in the

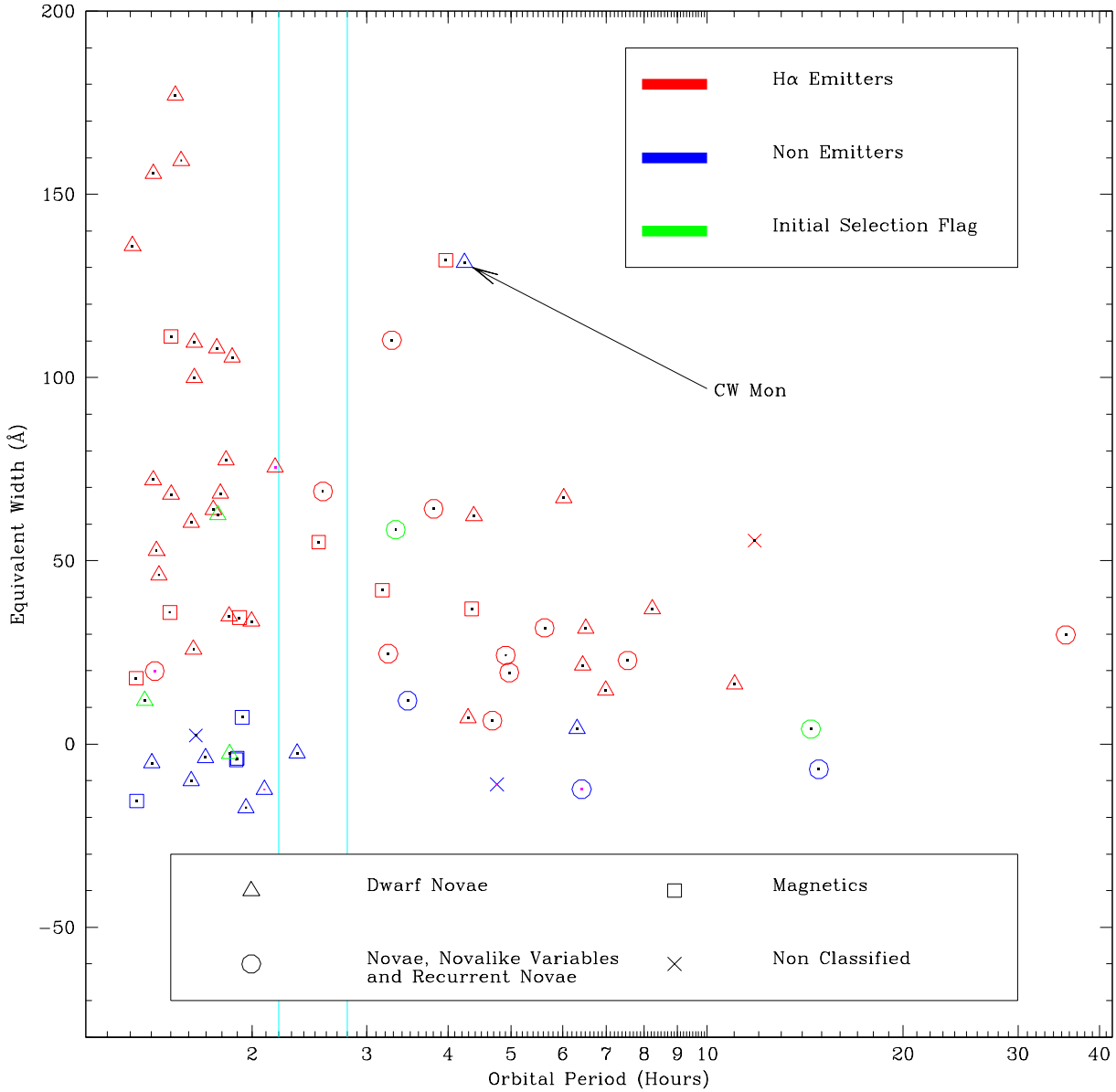


**Figure 5.** A plot of EW versus the orbital period of CVs in the Off-Plane and In-Plane samples. The orbital period gap is shown between the cyan lines.

figure legend and are used to distinguish between the CV types (symbols) and the emitters (colours). A small dot in the centre of each symbol refers to the data in the CV flag and CV Type column of table 1. The dot is coloured magenta if the CV flag is not equal to zero (the CV is not in the catalogue or it is of uncertain nature) or the CV type is of an uncertain nature. If the CV flag is zero and the CV type is certain, the dot is black.

The short-period quiescent DNe show the greatest EW, and the survey has no problems in detecting them as emission line objects. In fact the long-period nova V1425 Aql

shows the biggest EW but it misses our initial selection cuts and the EW estimate is too large to be physical, hence it is not shown in the figure. There are more short-period DNe than long-period DNe in our sample, which is a characteristic of the Ritter & Kolb catalogue as a whole (and expected on evolutionary grounds).

As already noted in section 5.1.2, long-period systems have a lower H $\alpha$  excess, but the survey is still sensitive enough to detect many of them as emitters. As shown in Fig. 5 the boundary between systems detected as emitters and those undetected corresponds to a H $\alpha$  EW of  $\sim 10\text{\AA}$ ;

the average excess for all systems is clearly above this value, irrespective of period. Thus most long-period CVs do exhibit photometrically detectable H $\alpha$  emission, albeit at a lower EW level than short-period systems.

There is one object in Fig. 5 that shows a large apparent H $\alpha$  EW, but was not selected as an emitter. This object is the long-period dwarf nova CW Mon, which is located in a field of poor data quality. In fact, this field does not meet the IPHAS criteria for inclusion in the final survey and will be re-observed. As a result, the stellar locus exhibits a large scatter which places the cut further up in the colour-colour plots compared to fields with good data quality. The CV is separated from the locus to the extent that, on our colour-colour plots, it appears above the graphical representations of the selection cuts. However, it is not selected due to the large uncertainties of the magnitudes. Past spectroscopic observations have revealed strong Balmer emission in CW Mon (Szkody 1987).

## 6.2 $r' - i'$ vs Orbital Period

In Fig. 6 we plot  $r' - i'$  colour against orbital period. No obvious correlation is seen, but we note that the  $r' - i'$  colours of the CVs in this plot span a range of more than 1 magnitude. Based on this, we believe the use of selection criteria based on this broad-band colour (such as a “blue cut”) would not be prudent in the construction of a new CV sample from IPHAS. In this context, it is also worth keeping in mind that the sample of known CVs analyzed here may already suffer from selection effects. It is therefore important to minimize the number of *a priori* selection criteria when constructing new samples that are meant to better represent the true CV parent population.

## 6.3 H $\alpha$ EW vs Absolute Magnitude

In order to test for a correlation between intrinsic brightness and EW, we calculated absolute magnitudes for CVs with known distances in our sample by assuming a galactic extinction law of  $A_V = 1.5$  mag/kpc. In doing so, we also assumed an  $R_V = 3.1$  extinction curve to convert  $A_V$  to  $A_{r'}$ . Fig. 7 shows the relationship between the resulting absolute magnitudes and our estimated EWs for various groupings.

In the plot showing all systems, there appears to be a correlation, albeit with large scatter. The existence of a correlation becomes more apparent when we plot the individual CV types separately. For the DNe and the novae, in particular, there is a definite trend for the H $\alpha$  EW to increase towards larger (that is fainter) absolute magnitudes. The magnetic systems do not show this trend, which is reasonable given the lack of accretion discs in the AM Her systems.

Our results agree qualitatively with the work of Patterson (1984), who has calculated a fit to the relationship between absolute magnitude and H $\beta$  equivalent widths. Note, however, that Patterson removed the contribution of the secondary from his absolute magnitude estimates and thus considered only the intrinsic brightness of the accretion disc in his correlation. We have not made this correction, nor have we corrected in any way for inclination. Nevertheless, all of our results clearly confirm that short-period, faint CVs (which are expected to represent the most numerous CV

population) exhibit the strongest H $\alpha$  emission lines. Thus photometric emission line surveys are indeed an excellent resource for finding and studying this population.

## 7 DISCUSSION

### 7.1 Prospects for CV Searches Based on Emission Line Surveys

A key question we wanted to address with this study was “can surveys like IPHAS find members of the postulated large population of faint, short-period CVs”? The results here confirm that short-period CVs generally exhibit relatively large H $\alpha$  excesses in IPHAS, so if the hypothesized large population of short-period CVs conform to this rule, the survey would have no problem detecting them. More surprisingly, we have also been able to recover long-period CVs as H $\alpha$  emitters with a comparable success rate. Thus we actually do not expect any additional bias from the survey in favour of detecting either long- or short-period CVs.

The vast majority of short-period systems are believed to be DNe. However, due to the low mass accretion rates in these systems, the outburst duty cycle is extremely low. For example, the proto-type WZ Sge erupts on average every 30 yrs and stays bright for only a few months. In the context of an emission line survey for CVs, this may actually be an advantage. The results here show that IPHAS is unable to detect most DNe in outburst via our selection method, whereas quiescent DNe tend to show the greatest H $\alpha$  excesses. Thus short-period DNe are actually more likely to be discovered by IPHAS if they have long outburst intervals.

It is interesting to ask how many faint, short-period CVs IPHAS might eventually discover. Given the low accretion rates and very low mass secondaries, it is possible that the optical luminosity of these systems will actually be dominated by their WD primaries. An accretion-heated WD in a short-period system would be expected to have an effective temperature of  $T_{eff} \simeq 10000$  K (Townsend & Bildsten 2003). IPHAS could see such an object out to 275 pc, given its limiting magnitude of  $r' = 19.5$ . For an assumed CV space density of  $5 \times 10^{-5} \text{pc}^{-3}$  (see discussion below), there are roughly  $\sim 0.1$  short-period CVs per square degree brighter than  $r' = 19.5$  mags near the galactic plane. Since IPHAS will image 1800 square degrees, we would predict that  $\sim 180$  of these systems could be detected with IPHAS.

This prediction is conservative in the sense that no active CV should be fainter than the estimate used above – any admixture of brighter CVs will increase the total number considerably (there are intrinsically fewer of these, but they can be seen to greater distances). The prediction does, of course, scale directly with the assumed space density. The number adopted above is based on theoretical population synthesis predictions (Kolb 1993), and is higher than most existing empirical estimates (Patterson 1998; Gänsicke 2005). This is not a problem, as it is precisely this discrepancy between theory and observation that an IPHAS CV sample would be designed to test.

It has already been noted in Section 5.1.4 that a faint CV will on average need to display a greater H $\alpha$  excess than a bright CV in order to be detected. However, if the trend

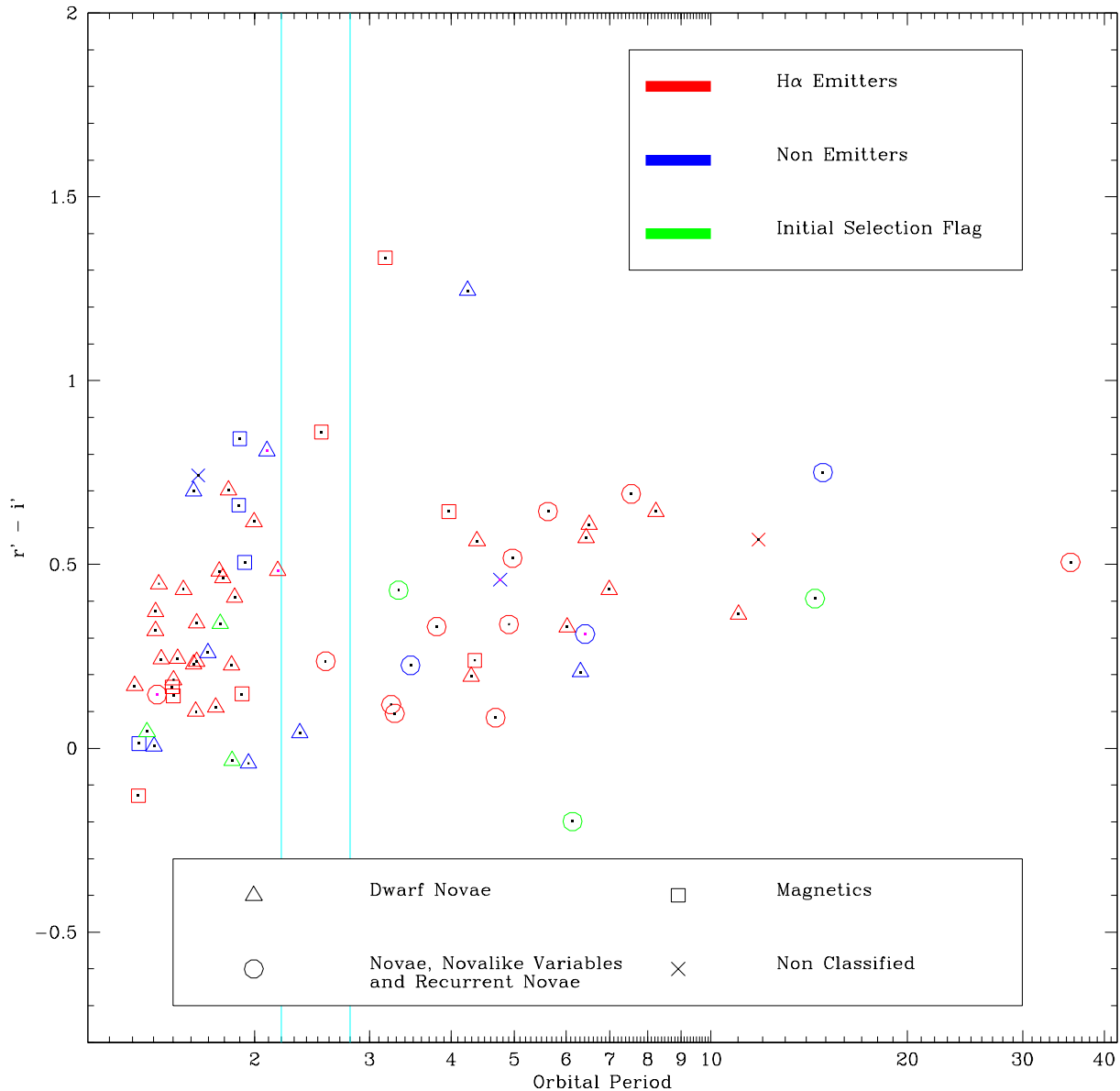


**Figure 6.** A plot of  $r' - i'$  versus the orbital period of CVs in the Off-Plane and In-Plane samples. The orbital period gap is shown between the cyan lines.

towards larger EWs for short-period, faint DNe continues to hold for this population, then there may be no problem in detecting these systems even close to the magnitude limit of the survey.

Considering all of the above, it seems clear that IPHAS (and similar surveys) does have the potential to test theoretical population synthesis predictions.

## 7.2 Implementing an IPHAS-based CV Search

Initial follow-up to the IPHAS survey has already led to many clear H $\alpha$  emitters being spectroscopically observed and identified. A key problem in constructing a new sample of CVs in this way is the presence of other large populations of objects displaying H $\alpha$  emission. Selecting objects for spectroscopic follow-up using the selection techniques illustrated here can uncover most of the CVs, but the fraction of CVs amongst objects selected in this way may not be large. Our results to date suggest that early type emission line stars (for example Be stars) tend to dominate bright ( $r' \lesssim 18$ )

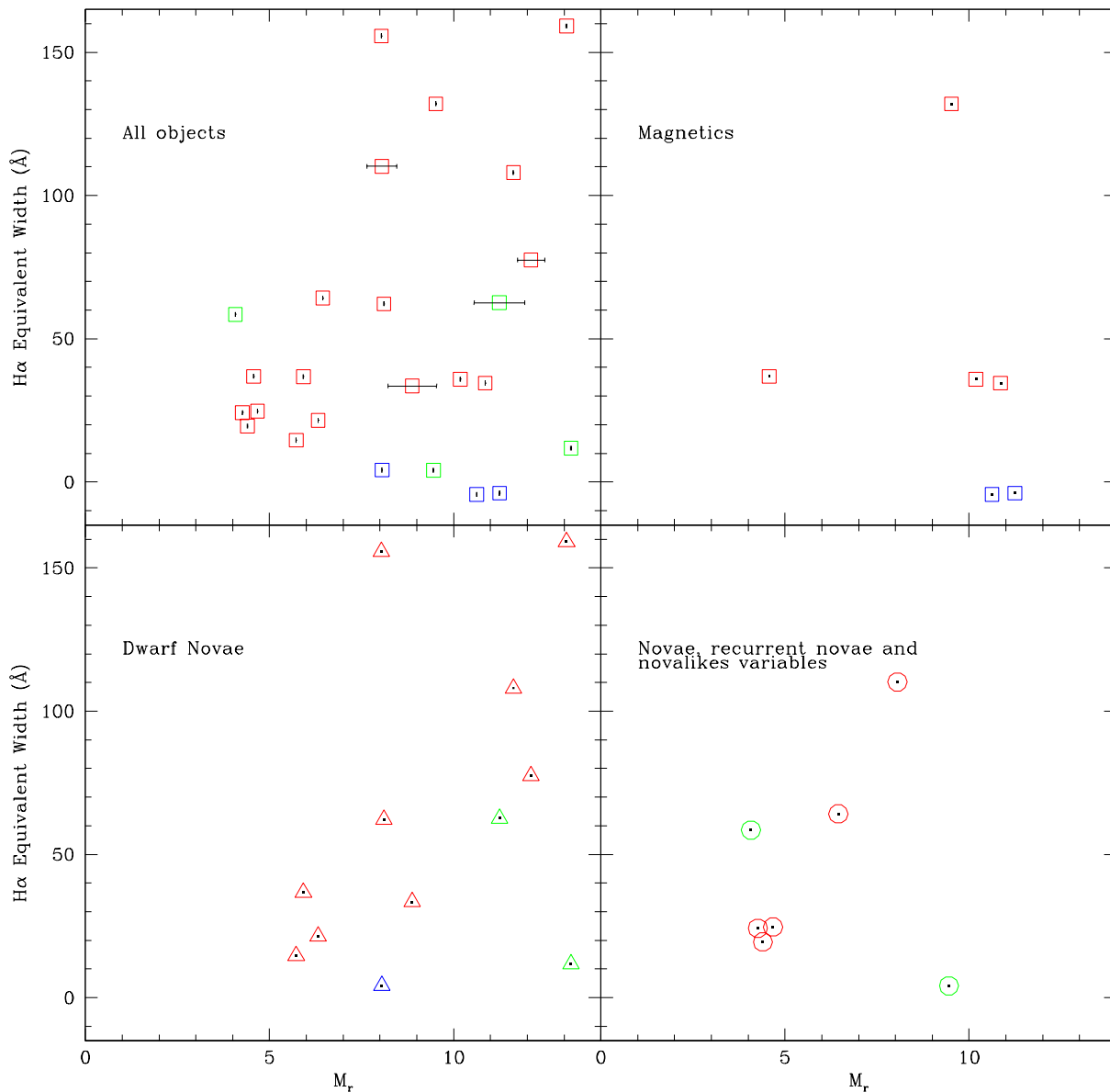


**Figure 7.** The relationship between the absolute magnitude and the  $H\alpha$  equivalent width for the CVs with known distances. The symbols are plotted in red if the systems is a  $H\alpha$  emitter; blue if it is a non-emitter; and green if it is a system which did not pass our initial selection cuts.

samples of  $H\alpha$  excess objects. Thus many non-CVs need to be observed in the process of constructing a new sample of CVs, unless the distribution of  $H\alpha$  excess objects changes significantly towards fainter magnitudes. We are currently investigating this possibility.

## 8 CONCLUSIONS

We have considered the properties of known CVs contained within the galactic plane  $H\alpha$  survey IPHAS as of July 2004,

along with those of a sample of CVs outside the galactic plane observed with the same observational setup. We have developed routines to select clear  $H\alpha$  emitters from the IPHAS photometry and used these routines to determine the percentage of CVs in our samples that would be recovered as  $H\alpha$  emitters.

We find that the overall completeness of IPHAS-like surveys for detecting CVs as emission line objects is  $\simeq 70$  per cent, roughly independent of CV type and orbital period. Our recovery fractions are steady near this value up to at least  $r' \simeq 18.5$  and only drop towards the very faintest

magnitudes we consider ( $r' = 19.5$ ). There are 23 CVs in our samples not recovered as H $\alpha$  emitters. Six do not pass our initial selection cuts, and 2 are without a known subtype. Several are not recovered due to observing some CVs when H $\alpha$  emission is expected to be weak or absent, for example DNe in outburst, and magnetic CVs in a low state. The remainder of non-recovered CVs are due to scatter in faint magnitude bins and cases where the fitting process did not produce good results.

We have estimated H $\alpha$  EWs from our photometry and find that, as expected, short-period CVs show the strongest H $\alpha$  emission lines. This is encouraging for the prospects of finding the predicted population of faint, short-period CVs. However, we also find that most long-period CVs exhibit strong enough H $\alpha$  emission for them to be easily detected by IPHAS-like surveys.

In closing, we expect that IPHAS (and related surveys) will allow us to construct samples of CVs that are free from most of the selection effects that have plagued previous comparisons between theoretical population synthesis predictions and observations. In particular, such samples should uncover the long-predicted large population of faint, short-period systems, if it exists.

## ACKNOWLEDGMENTS

Based in part on observations made the Isaac Newton Telescope, which is operated on the island of La Palma by the Isaac Newton Group in the Spanish Observatorio del Roque de los Muchachos of the IAC. ARW was supported by a PPARC Studentship. BTG was supported by a PPARC Advanced Fellowship. DS acknowledges a Smithsonian Astrophysical Observatory Clay Fellowship.

## REFERENCES

- Aungwerojwit, A., et al., 2005, *A&A*, 443, 995  
 Cropper, M., 1990, *Space Science Reviews*, 54, 195  
 Dhillon, V. S., 1996, in *ASSL Vol. 208: IAU Colloq. 158: Cataclysmic Variables and Related Objects*, p. 3  
 Downes, R. A., Webbink, R. F., Shara, M. M., Ritter, H., Kolb, U., Duerbeck, H. W., 2001, *PASP*, 113, 764  
 Drew, J. E., et al., 2005, *MNRAS*, 362, 753  
 Ferrario, L., Wickramasinghe, D. T., 1993, *MNRAS*, 265, 605  
 Gänsicke, B. T., 2005, in *ASP Conf. Ser. 330: The Astrophysics of Cataclysmic Variables and Related Objects*, p. 3  
 Gänsicke, B. T., Hagen, H.-J., Engels, D., 2002, in *ASP Conf. Ser. 261: The Physics of Cataclysmic Variables and Related Objects*, p. 190  
 Howell, S. B., Rappaport, S., Politano, M., 1997, *MNRAS*, 287, 929  
 Kamath, U. S., Anupama, G. C., Ashok, N. M., Chandrasekhar, T., 1997, *AJ*, 114, 2671  
 Kolb, U., 1993, *A&A*, 271, 149  
 Kube, J., Gänsicke, B. T., Euchner, F., Hoffmann, B., 2003, *A&A*, 404, 1159  
 Munari, U., Zwitter, T., Bragaglia, A., 1997, *A&AS*, 122, 495  
 Patterson, J., 1984, *ApJS*, 54, 443  
 Patterson, J., 1998, *PASP*, 110, 1132  
 Ritter, H., Kolb, U., 2003, *A&A*, 404, 301  
 Shara, M. M., Livio, M., Moffat, A. F. J., Orio, M., 1986, *ApJ*, 311, 163  
 Szkody, P., 1987, *ApJS*, 63, 685  
 Townsley, D. M., Bildsten, L., 2003, *ApJ*, 596, L227  
 Warner, B., 1987, *MNRAS*, 227, 23  
 Warner, B., 1995, *Cataclysmic variable stars*, Cambridge Astrophysics Series, Cambridge, New York: Cambridge University Press, —c1995  
 Williams, R. E., 1980, *ApJ*, 235, 939

This paper has been typeset from a  $\text{\TeX}/\text{\LaTeX}$  file prepared by the author.